J. Fluid Mech. (1974), *vol.* 63, *part* 1, *pp.* 121–144
Printed in Great Britain

Mean and fluctuating flow measurements in the hypersonic boundary layer over a cooled wall

By A. J. LADERMAN AND A. DEMETRIADES

Philco-Ford Corporation, Newport Beach, California

(Received 29 May 1973)

Measurements of the mean flow, intermittent structure and turbulent fluctuations were made in a cold-wall boundary layer at a stream Mach number of 9·4 and Reynolds number based on momentum thickness of 36800. For these conditions, the r.m.s. sublayer thickness was 32 times smaller than that of the boundary layer proper, and the interfacial standard deviation of the latter was about three times proportionately smaller than has been found at low speeds. The mean flow data, which extended well into the sublayer, revealed a large increase in static pressure from the layer edge to the wall and a quadratic law relation between the total temperature and velocity. While the transformed velocity profile was in good agreement with the incompressible law of the wake, no indication of a linear variation of velocity in the sublayer was detected.

Hot-wire fluctuation data, interpreted with the use of appropriate assumptions concerning the nature of the sound field, indicated that the turbulence is dominated by high-frequency pressure fluctuations whose magnitude at the wall and beyond the layer edge agree with extrapolation of data acquired at supersonic speeds. The static temperature fluctuations agreed with expectations from adiabatic, supersonic data apparently because they were suppressed by the cooled-wall condition. The fluctuations in the longitudinal velocity component were generally small and differed little from lower Mach number results. The high turbulence Reynolds numbers found generated an inertial-subrange spectral decay, while the longitudinal integral scales were found independent of turbulence mode and about one-fifth the boundary-layer thickness.

1. Introduction

The turbulence structure of high speed boundary layers has gained considerable importance since the measurements of Kistler (1959) first charted the distribution of fluctuation intensities with distances from the surface at Mach numbers from 1·7 to 4·8. At these supersonic speeds compressibility makes drastic changes in the nature of the turbulent flow. The disturbances are mostly composed of density and temperature fluctuations; velocity fluctuations begin decreasing in significance. Kistler demonstrated that the adiabatic relation $T' = (\gamma - 1) M^2 u'$ holds, and that T' reaches a maximum value in the boundary layer which depends on the 'driving force' $T_{0e} - T_e$. For adiabatic flows the latter temperature difference depends only on the external Mach number M_e; for $M_e \to \infty$ the fluctuation

T' appears to reach a value of about 0·16. According to the adiabatic relation, u' then becomes vanishingly small. At high hypersonic speeds one would therefore expect that the slightest local velocity change of a fluid particle would cause large changes in its temperature. In the limit one formally visualizes a turbulent boundary consisting of essentially nothing but entropy 'spots'.

Of more immediate interest, however, is the turbulent structure in the range $5 < M_e > 15$. Here one proceeds from a range where compressibility effects have become important to one where these effects are dominant. In this range, too, another possibly dominant factor appears in the form of pressure fluctuations p' as indicated by extrapolation of the fluctuating wall pressure measurements made by Kistler & Chen (1963), as well as those carried out in the flow beyond the edge of the boundary layer by Laufer (1964). These two levels are expected to be, say at $M_e = 10$, about $p' = 10$–$15\,\%$ and $3\,\%$, respectively. Viewed in the background of our earlier remarks on the decreasing u', the pressure (sound) mode looms much more prominent than vorticity at hypersonic speeds.

The expected importance of the pressure fluctuations generates a severe practical difficulty. In an overall sense, the hot-wire anemometer remains the most convenient diagnostic tool for hypersonic turbulence experimentation, but it is well known that a complete 'modal analysis' is in principle impossible with this anemometer in the presence of pressure fluctuations. In fact the assumption $p' \equiv 0$ has been exclusively used in the few turbulence measurements reported at supersonic speeds. At the very least, the hot-wire technique cannot be straightforward when turbulent boundary layers are probed at elevated Mach numbers. The present experiment is aimed at measuring the turbulence intensities in a hypersonic boundary layer, with a view to resolving some of the questions posed above.

2. Notation

In the following, the pressure, velocity, density and temperature of the flow are represented by the usual notation p, u, ρ and T, respectively. The entropy, vorticity and sound modes are identified by the symbols σ, τ and π. For any fluctuating variable s we have defined Δs as the instantaneous fluctuation in s, $\bar{s}$ as the mean value of s, and s' as its r.m.s. value normalized by the local mean. Conditions at the wall, at the boundary-layer edge and in the free stream are denoted by the subscripts w, e and ∞, respectively, while the stagnation condition is indicated by the subscript 0. Other symbols are defined as they appear in the text.

3. Test facility, instrumentation and procedure

The experiment was carried out in the continuous flow, 21 in. hypersonic wind tunnel at the Jet Propulsion Laboratory in Pasadena, California. Measurements were made in the boundary layer growing over the upper wall (ceiling) of the 21 in. high × 20 in. wide test section, in a vertical plane located at the tunnel mid-span and at a station 160 in. downstream of the nozzle throat. Conditions

of the test were: Mach number $M_\infty = 9{\cdot}4$; total pressure $p_0 = 3200$ cmHg; total temperature $T_{0e} = 1000\,°\text{F}$ (810 °K); wall temperature $T_w = 100\,°\text{F}$ (310 °K); and Reynolds number $Re_\infty = 127\,000\,\text{cm}^{-1}$.

Local mean flow properties were determined from measurements made with a Pitot probe, a static pressure probe and a total temperature thermocouple, while turbulence measurements were made with the hot-wire anemometer operated in the constant-current mode. The probes, 3 in. apart, were mounted on an instrumentation rake, with their sensing tips lying on a straight line normal to the flow and parallel to the wall surface. The rake, shown in figure 1 (plate 1), was suspended on a remotely controlled actuator mechanism by means of which the distance y between the wall and probes could be fixed with a precision of 0·001 in. (0·0025 cm) (amounting to $0{\cdot}25 \times 10^{-3}\,\delta$) over a total stroke of 8 in. (20 cm). Resolution in the $\delta = 4$ in. (10 cm) thick boundary layer was at worst controlled by the Pitot tube openings of $\frac{1}{8}$ in. ($\frac{1}{32}\delta$). To improve the resolution of the Pitot survey in the sublayer (of order $\delta_s = 0{\cdot}10$ in. thick) a miniature Pitot probe was made of a flattened tube with an opening 0·008 in. high ($= \frac{1}{12}\delta_s$) and 0·060 in. wide. Three Pitot measurement stations, located at the rake centre and at 6 in. on either side of the centre, were used to check flow two-dimensionality across the 21 in. span of the wind-tunnel test section. Static pressure measurements were made in the boundary layer, using a sharply pointed 0·050 in. diameter tube, aligned in the direction of flow, with three sensing holes 0·015 in. diameter located 0·75 in. from its tip. Static pressures were also recorded on the wall in the vicinity of the rake measurements.

Both Pitot and static pressure measurements were examined for corrections due to various probe errors and, while the latter had to be corrected for large viscous interaction effects (described in §4), the influence of thermal creep and vibrational degree-of-freedom effects were found to be negligible. Viscous (Kane & Maslach 1950; Mathews 1958) and rarefaction effects (Rogers, Wainwright & Touryan 1966) on the response of the Pitot pressure probe were sufficiently small to ignore.

The total temperature probe consisted of a type J iron–constantan thermocouple. Its leads were inserted through, and cemented in, a $\frac{3}{32}$ in. diameter alumina tube, which was then installed in the $\frac{1}{8}$ in. O.D. copper tube located on the instrumentation rake. The alumina body was notched and the adjacent tube wall grooved, so that the thermocouple could be held in position by a spring clip inserted over the tube. The thermocouple junction was positioned $\frac{7}{16}$ in. from the opening of the copper tube, and three 0·031 in. diameter vent holes were drilled through the tube wall at this same location. The total temperature probe was calibrated in a stream at Mach 9·5 and 6 and 1000 °F (810 °K), and also at Mach 4 with stagnation temperatures ranging from 80 to 1000 °F (300 to 810 °K). The probe recovery factor, defined as the ratio of measured to actual stagnation temperature, was found to depend almost exclusively on the Reynolds number based on probe diameter and stagnation temperature.

The hot-wire anemometer, shown in figure 2 (plate 2), consisted of a 0·00001 in. (25×10^{-6} cm) diameter Pt 10 % Rh wire mounted across the tips of two sharp-pointed prongs. The wires were mounted with sufficient slack to eliminate spuri-

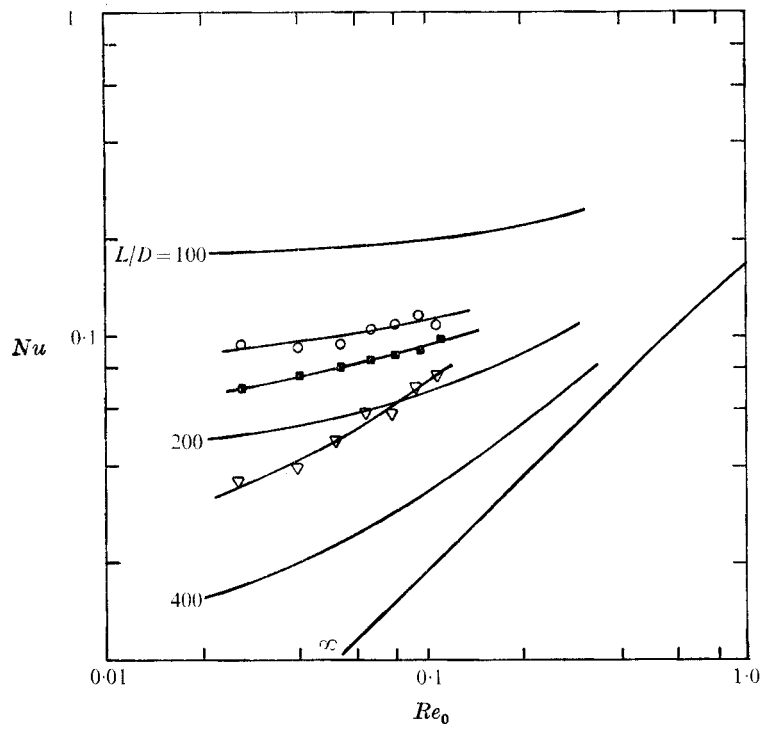

FIGURE 3. Heat-transfer characteristics of typical hot-wire probes. ——, theory ($\eta_{prong} = 0{\cdot}9$), indicating the effect of end losses for wires of finite aspect ratio.

	Wire no.	L/D	α_r
○	6–3	358	0·0013
■	2–5	265	0·0016
▽	A 13–1	390	0·0015

ous signals due to 'strain-gauge' effects. For the wires used in these experiments, the aspect ratio ranged from 200 to 400. The probe body consisted of a $\frac{3}{32}$ in. diameter $\times 1\frac{1}{4}$ in. long alumina cylinder. A $\frac{1}{32}$ in. diameter $\times \frac{1}{4}$ in. long alumina cylinder, used to support the 3 mm diameter hot-wire prongs, was cemented to one end of the larger cylinder at an angle of approximately 20–30°. Details of the probe construction, including the technique for bonding the hot-wire element to the prongs with gold paint, were described by Doughman (1972).

Following the hot-wire probe assembly, the temperature-resistance behaviour of each probe used was measured in a controlled oven over the range from 60 to 300 °F (290–470 °K). The heating due to these currents is small, so that hot-wire resistance R could be expressed as a linear function of the square of the current i. The zero current resistance was then obtained by extrapolation yielding a curve of R against temperature T:

$$R = R_r[1 + \alpha_r(T - T_r)], \tag{1}$$

where $T_r = 273$ °K† and R_r are reference conditions. Typical values of α_r were found to be $1{\cdot}4$–$1{\cdot}5 \times 10^{-3}\,\mathrm{K}^{-1}$.

† From initial calibrations up to 800 °K, it was found that the second coefficient of resistivity was zero.

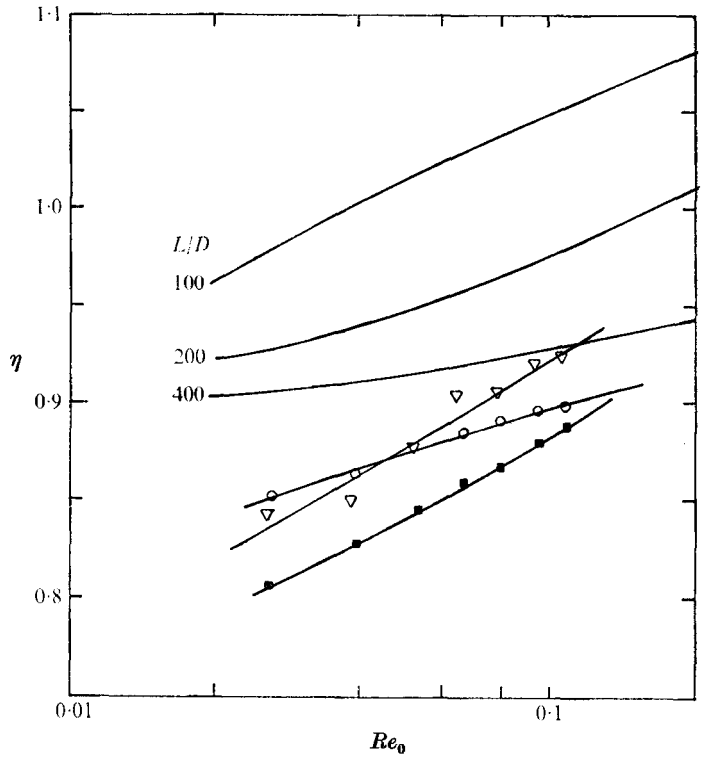

FIGURE 4. Recovery temperature characteristics of typical hot-wire probes. ——, theory ($\eta_{prong} = 0{\cdot}9$).

	Wire no.	L/D	α_r
○	6–3	358	0·0013
■	2–5	265	0·0016
▽	A13–1	390	0·0015

Immediately prior to its use in the wind tunnel, each probe was 'flow-calibrated' to determine its heat-transfer characteristics. This was done by locating the wire in the wind-tunnel free stream, where the flow conditions are well known, and varying the Reynolds number by setting the tunnel total pressure at specific values between 700 and 3200 cm Hg. At each pressure the derivative $\partial R/\partial i^2$ was found from the slope of the R against i^2 curve obtained by operating the wire at 8 overheat currents. The Nusselt number at zero overheat Nu_0 was then given by

$$Nu_0 = \frac{\alpha_r R_r}{\pi l k_0} \frac{R_{aw}}{\partial R/\partial i^2}, \tag{2}$$

where $\alpha_r R_r$ and the wire length l were obtained from the oven calibration, k_0 is the thermal conductivity of air evaluated at T_0, and R_{aw} is the adiabatic resistance found by extrapolating the calibration curve to zero current. The recovery factor, $\eta \equiv T_{aw}/T_0$, where T_{aw} is the adiabatic wire temperature, was computed by using R_{aw} to obtain T_{aw}.

Typical flow calibration curves are shown in figures 3 and 4, which also include theoretical expectations for aspect ratios ranging from 100 to infinity. Because of the low Reynolds numbers, it is seen that large end losses are to be expected.

However, the agreement between theory and experiment is observed to be very poor, probably because the basic assumptions of the theory (e.g. straight wires, no flow interference by the prongs, etc.) are not satisfied by the actual probes. The calibration procedure has the basic advantage, therefore, of avoiding reliance on purely theoretical means for predicting the hot-wire heat-transfer characteristics. The calibration curves shown in figures 3 and 4 were put into the following analytical form for use in the data reduction process:

$$\left.\begin{aligned} Nu_0 &= A_1 + A_2 Re_0^{\frac{1}{2}} + A_3 Re_0, \\ \eta &= B_1 + B_2 Re_0^{\frac{1}{2}} + B_3 Re_0, \end{aligned}\right\} \tag{3}$$

where Re_0 is the Reynolds number based on the hot-wire diameter, and T_0 and the coefficients A_i and B_i were determined from a least-squares curve fit to the data.

It should be of interest to note that these wires of 0·00001 in. (0·000025 cm) diameter, with aspect ratios as high as 500, showed a good record of survival in the flow, in which dynamic pressures of order 5 cmHg at 1000 °F (810 °K) were encountered. The experiment required that the data collecting probe withstand the environment for several hours at a time. It was not uncommon to meet and exceed this performance. Finally, the 'boundary-layer frequency' u_e/δ was about 10 kHz, considerably below the limit of the compensated constant-current circuitry of the measuring and recording system. A complete 'library' of the wire signals was created on an FM tape recorder at each point in the flow.

The determination of the r.m.s. fluctuations of the flow variables (or modes) and their cross-correlation coefficients can be accomplished using the method of modal analysis developed by Kovasznay (1950), Morkovin (1956) and their co-workers. For example, since the hot wire responds directly to mass flux and total temperature variations in the flow, the r.m.s. output from the wire is related to the r.m.s. fluctuation in mass flux $m' = [\overline{(\Delta\rho u)^2}]^{\frac{1}{2}}/\overline{\rho u}$, the r.m.s. total temperature fluctuation $T_0' = [\overline{(\Delta T_0)^2}]^{\frac{1}{2}}/\overline{T_0}$, and their cross-correlation coefficient R_{mT}. Consequently, operating the hot wire at three heating currents yields three equations, which can be solved for the unknowns m', T_0' and R_{mT}. The accuracy of this method can be increased significantly, if more than three measurements are made; and fifteen values of heating current were chosen in the present experiment. The highly redundant system of fifteen equations was then solved by the method of least squares.

Turbulence measurements were made at over 40 locations y in the boundary layer. At each point the wire was operated at the fifteen overheat currents described above and both the mean and fluctuating voltages were recorded on magnetic tape. Just before the measurements, the hot wire was located in the free stream, and its time constant was measured at a known current using the square-wave method. The compensating amplifier was then adjusted to that value of the time constant for the remainder of the test; the purpose of this procedure is clarified in §6. Mean flow measurements were also made at a total of 73 positions within the boundary layer, including the 40 turbulence measuring stations. Finally, detailed intermittency measurements were made at closely spaced y points in the neighbourhood of the sublayer and boundary-layer edges.

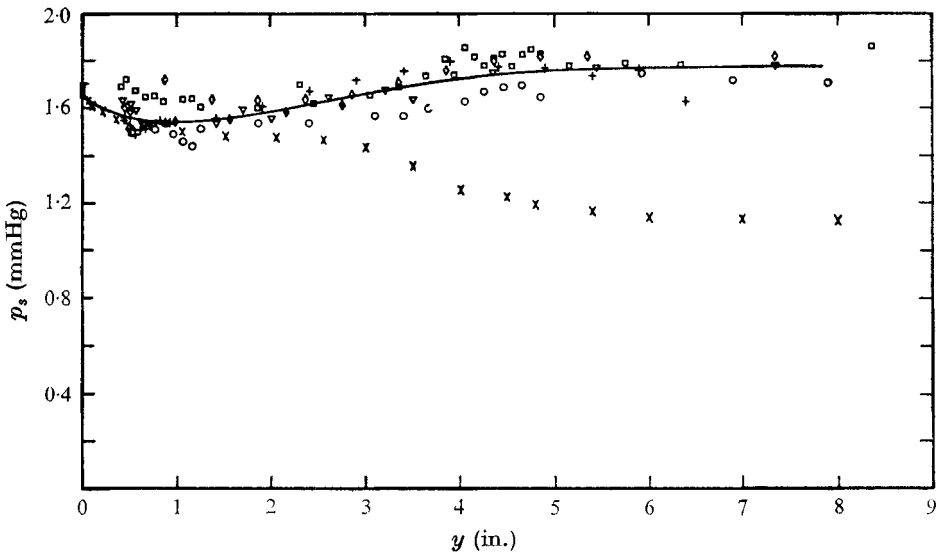

FIGURE 5. Static pressure variation through the boundary layer. For calculation of the mean flow, the measured pressures were replaced by the polynomial curve fit to the data (——). ×, calculated p_s

Measured p_s	◇	◆	□	▽	○	+
Run	2	6	10	11	14	15

In this paper we shall describe the hypersonic boundary-layer structure from three viewpoints. Section 4 presents the mean flow data which have interesting features in themselves, and which were needed to compute the hot-wire sensitivities to the various fluctuations. The intermittency structure, which delineates the sublayer and boundary-layer regions will be shown in §5. Finally, the turbulent fluctuations themselves are discussed in §6.

4. The mean flow properties

The final data reduction of the mean flow properties used the data from the centre Pitot tube, the static pressure probe and the total temperature probe. The 'outboard' Pitot probes were used primarily to make frequent checks on the two-dimensionality of the boundary-layer flow.† In addition, there were no significant Pitot-pressure differences between the larger Pitot probes on the rake and the miniature Pitot probe which, as noted in §3, was used to probe the sublayer region. The total temperature thermocouple readings were equally repeatable.

The static pressure data, presented in figure 5, showed considerably more scatter. A fifth-degree polynomial, fitted to these data by the least-squares method, was used to represent the static pressure variation. Although the static pressure probe gave a reading $p_{sm} \simeq 1{\cdot}8$ mmHg in the free stream, the static

† Laufer *et al.* (1971, private communication) showed that the boundary-layer flow was two-dimensional, repeatable and free of significant streamwise gradients.

Mean flow properties		
$P_0 = 3200$ cmHg	$T_w/T_{0e} = 0{\cdot}384$	$Re_e = 127{,}080\,\text{cm}^{-1}$
$T_{0e} = 792$ °K	$P_{se} = 1{\cdot}17$ mmHg	$Re_\theta = 36\,800$
$T_w = 304$ °K	$u_e = 1{,}225\,\text{ms}^{-1}$	$\delta^* = 2{\cdot}29$ in. (5·7 cm)
$T_e = 43$ °K	$M_e = 9{\cdot}37$	$\theta = 0{\cdot}29$ in. (0·72 cm)

Intermittent structure	
$\bar{\delta} = 4{\cdot}05$ in. (10 cm)	$d = 0{\cdot}276$ in. (0·7 cm)
$\bar{\delta}_s = 0{\cdot}125$ in. (0·32 cm)	$d_s = 0{\cdot}075$ in. (0·19 cm)

TABLE 1. Summary of boundary-layer structure.

pressure p_{si} calculated from the free-stream Pitot pressure and the supply pressure was 1·17 mmHg. This difference was attributed to viscous interaction effects on the static pressure probe. To account for this interaction, the ideal (actual) static pressure p_{si} was found from the measured pressure p_{sm}, using the viscous interaction correlation

$$p_{sm}/p_{si} = 1 + C_1\chi + C_2\chi^2,$$

where C_1 and C_2 are constants and

$$\chi = M^2/(C/Re_p)^{\frac{1}{2}}, \quad C = (\mu_w/\mu_\infty)\,(T/T_w).$$

The Reynolds number Re_p in the above expression is based on the distance between the tip of the probe and the pressure orifice. The constants C, C_1 and C_2 were found by combining results reported by Behrens (1963), who used a probe of almost identical geometry, with data obtained in these experiments to give

$$p_{sm}/p_{si} = 1 + 0{\cdot}0457\chi + 0{\cdot}0622\chi^2. \tag{4}$$

When applied to the readings of the static pressure probe, this formula disclosed the existence of a significant pressure gradient normal to the surface as indicated in figure 5. Such a pressure gradient is apparently common in the hypersonic boundary layers (Kemp & Owen 1972) observed on aerodynamic models, as well as nozzle walls, although its origin is unknown. When included in the data reduction, it had a substantial effect on the distribution of the mean flow properties, particularly near the wall.

Calculation of the mean flow properties was carried out using the measured Pitot pressure, total temperature and static pressure iteratively corrected for probe effects. Results are tabulated in table 1, and are shown in figures 6 and 7. The stagnation and static temperature profiles, figure 6, have been normalized with respect to the stagnation temperature at the edge of the boundary layer, T_{0e}.† The inset in figure 6 shows the region near the wall plotted to an expanded y scale. Since temperature measurements could not be made for $y < 0{\cdot}063$ in. (0·15 cm), the variation of T_0 in this region was represented by a third-degree polynomial curve fit to the data at $y = 0$ (where T_0 = the wall temperature T_w),

† In table 1 and figures 6–8, the mean flow edge properties were selected as the conditions at $y = 6$ in., beyond which the free-stream flow was essentially uniform.

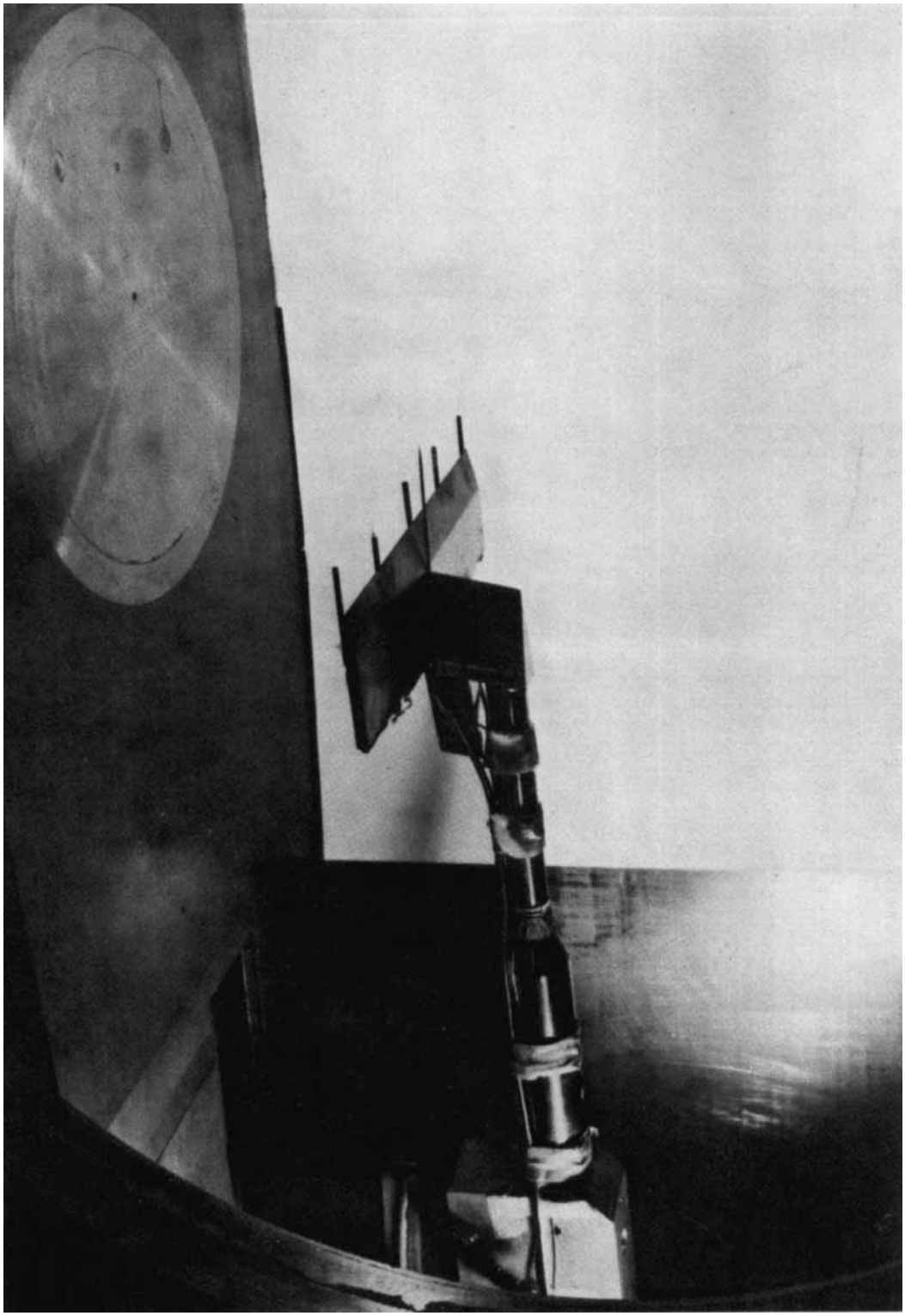

FIGURE 1. Instrumentation rake installed in test section of JPL hypersonic wind tunnel.

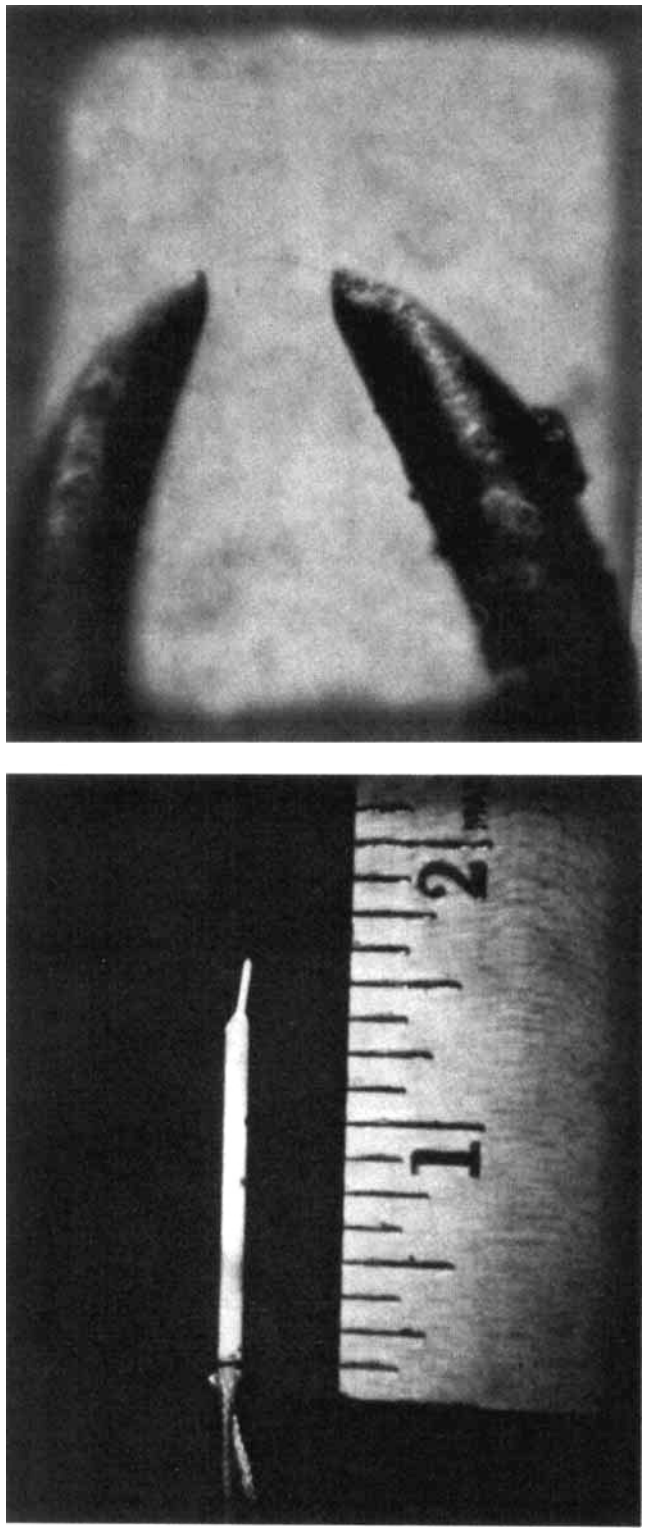

FIGURE 2. Hot-wire anemometer. View at right shows 0·00001 in. (0·000025 cm) diameter Pt 10 % Rh wire, mounted on 3 mm diameter Ni prongs. Wire aspect ratio is approximately 300 to 1.

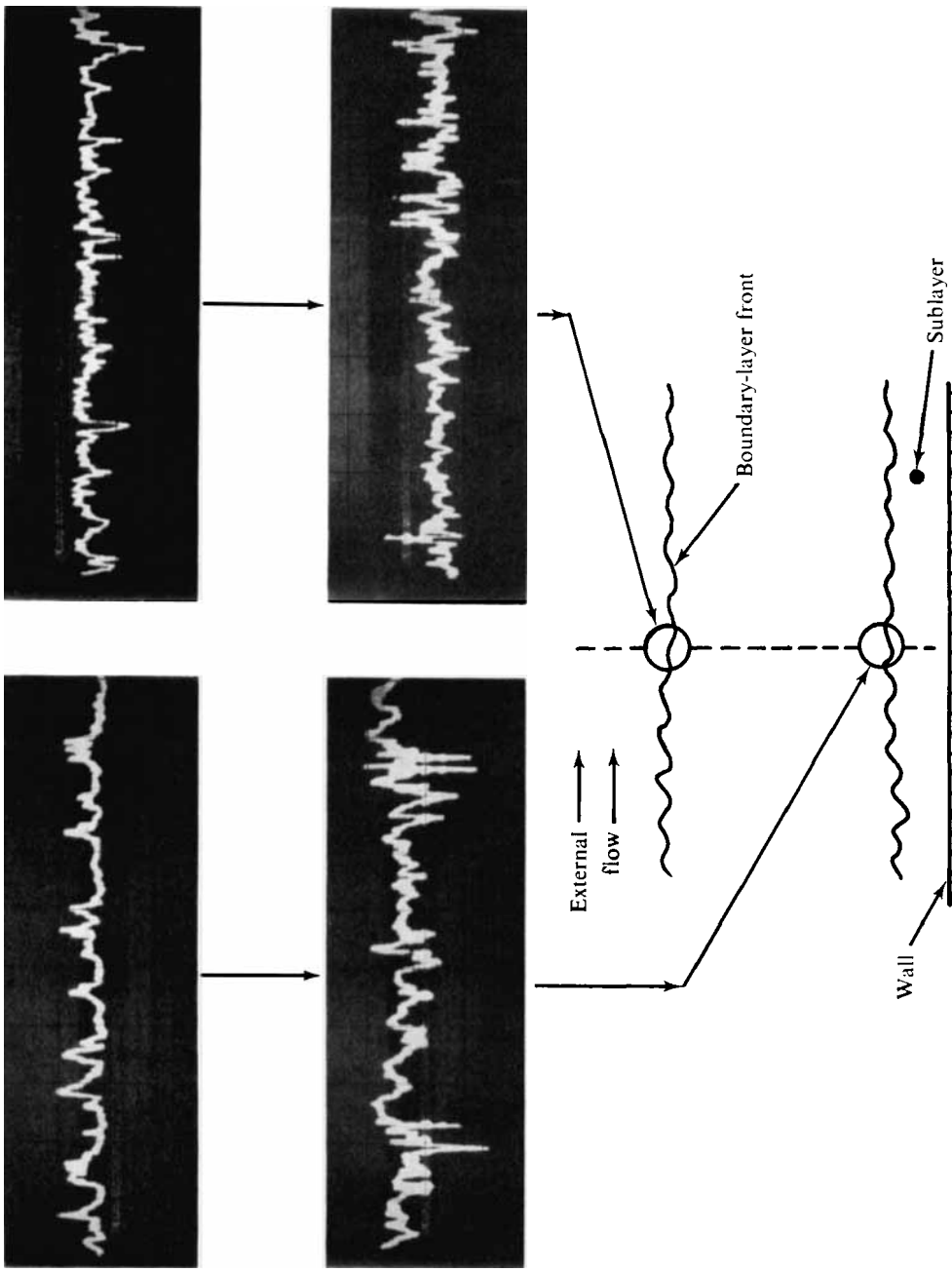

FIGURE 10. Hot-wire signal reversal in the intermittent zones. Both traces at left were recorded at the same point on the sublayer front ($y/\bar{\delta} = 0{\cdot}027$); those at right at the same point near the boundary-layer front ($y/\bar{\delta} = 0{\cdot}95$). For the top two traces the wire overheat was low (total-temperature sensitive); for the bottom two it was high (mass-flux sensitive).

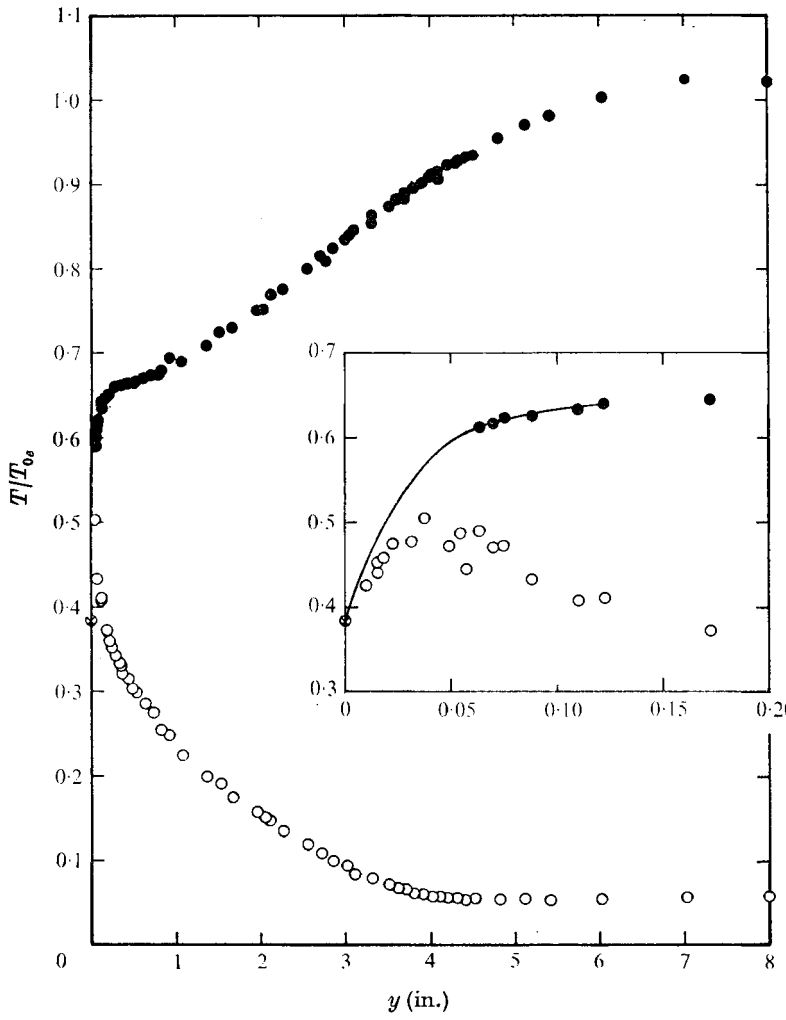

FIGURE 6. Variation of mean total and static temperatures through the boundary layer. Inset shows expanded view of temperature profiles near the wall and indicates static temperature overshoot (——, curve fit). $T_{0e} = 792\,°\text{K}$. Variable p_s: ●, T_0/T_{0e}; ○, T/T_{0e}; ⊗, T_w/T_{0e}.

and at y ranging from 0·063 to 0·122 in. (0·15–0·3 cm). The resulting static temperature profile T/T_{0e} shows the anticipated temperature overshoot, and indicates that the maximum static temperature occurs at $y \approx 0{\cdot}04$ in. (0·1 cm), well within the sublayer, where it exceeds the wall temperature by 140 °F (80 °K).

The velocity profile of figure 7, shows that over one half the change in velocity occurs in the immediate vicinity of the wall, i.e. $y < 0{\cdot}20$ in. (0·5 cm). This region, plotted with an enlarged y scale in the inset of figure 7, shows no evidence of the linear variation of velocity generally attributed to the viscous sublayer. The lack of a linear velocity profile in the presence of a cold wall was attributed by Walz (1962) and Lee, Yanta & Zeonas (1969) to the temperature overshoot that

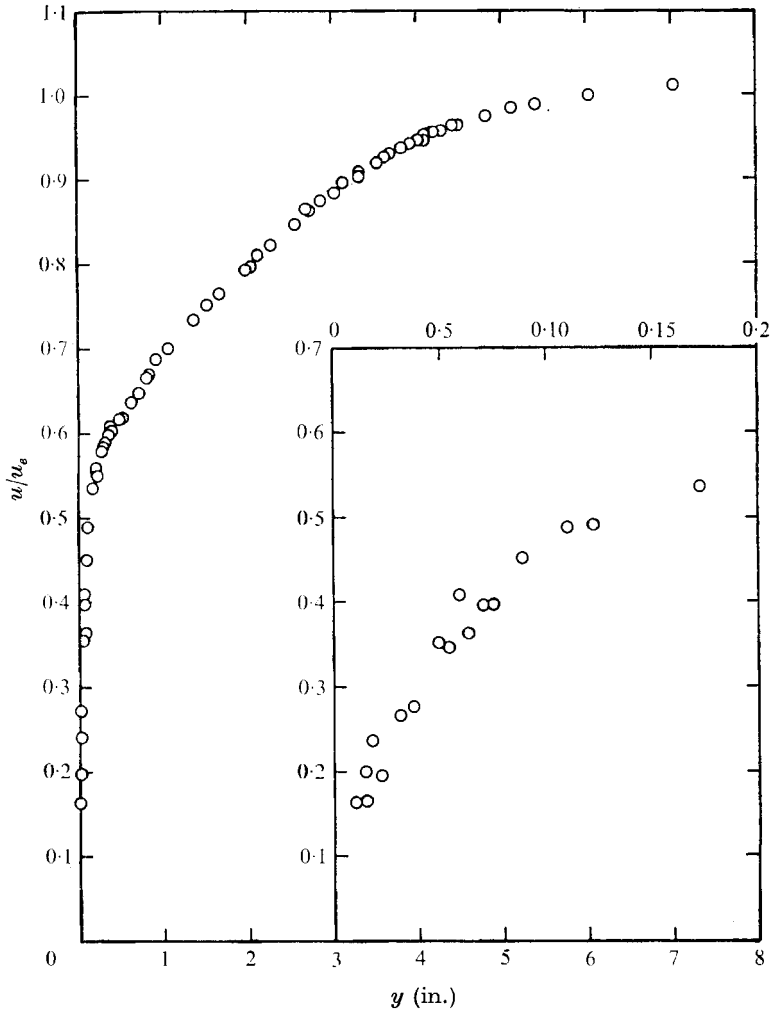

FIGURE 7. Non-dimensional mean velocity profile. Insert shows expanded view of velocity variation near the wall.

occurs adjacent to the surface. They reasoned that, if the shear stress is to remain constant in the sublayer, then the velocity gradient must compensate for variations in the viscosity arising from the temperature distribution. This would lead to a nonlinear velocity profile near the wall, and may account, in part, for the behaviour of the data observed in figure 7.

To assess whether the boundary layer was fully developed, the total enthalpy ratio $\tilde{T} = T_0 - T_w/(T_{0e} - T_w)$ was plotted against u/u_e, as shown in figure 8. In these co-ordinates, the Crocco relationship, which is valid for arbitrary heat-transfer rate and zero pressure gradient, is represented by the linear function $\tilde{T} = u/u_e$. In the sublayer the data agree with the theory, while in the outer portion of the boundary layer, corresponding to the law-of-the-wake region, the data follow closely the quadratic relation $\tilde{T} = (u/u_e)^2$. The interior of the boundary layer (the so-called law-of-the-wall region) is characterized by a well-defined

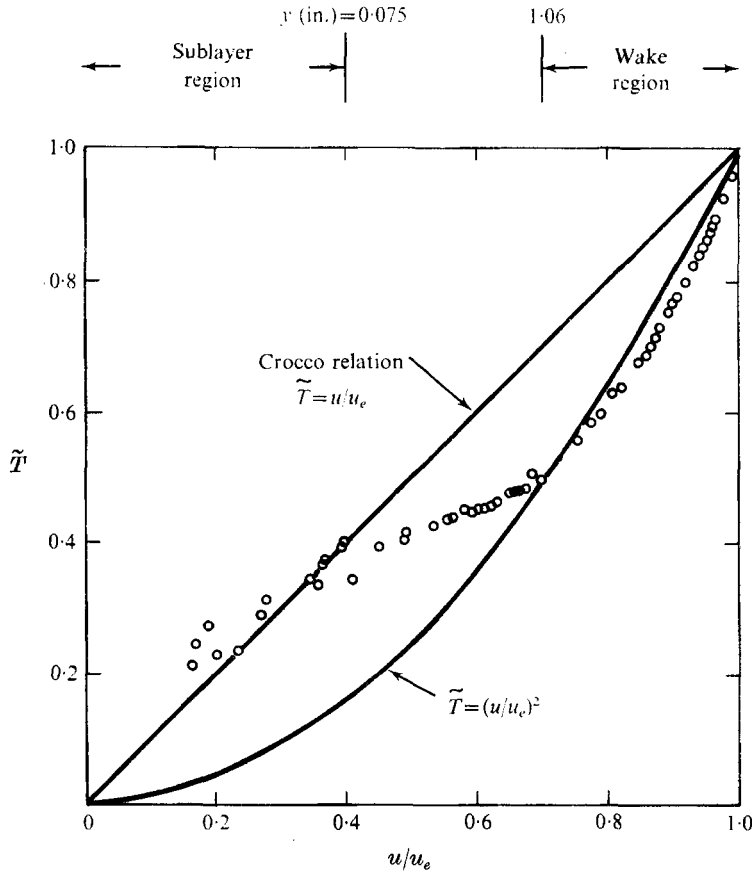

FIGURE 8. Non-dimensional total temperature–velocity profile.

transition between the linear and quadratic behaviour of the $\tilde{T}$ against u/u_e relationship. The total enthalpy profile of figure 8, particularly in the wake region, is typical of that obtained from measurement on cooled nozzle walls.

As will be seen later, the turbulence Reynolds number was very large, and the spectra showed the inertial-range behaviour characteristic of equilibrated boundary layers. Departures from the Crocco relation cannot, therefore, be due to low Reynolds number (non-equilibrium) effects. This is substantiated by the measurements of Feller (1973), which indicate that the quadratic relation may not be an inate characteristic of hypersonic tunnel wall boundary layers, but is rather associated with the wall temperature distributions common to hypersonic tunnels with unheated walls.

To examine further the nature of the boundary layer, the velocity profile of figure 7 was correlated with the 'universal' incompressible profile, using a procedure developed by Maise & McDonald (1968) for adiabatic flat plates and extended by R. Gran (1971, private communication) to include the cold-wall condition. The procedure involves fitting the data to the expression for the law of the wake, which, following Coles (1969), has been re-written in the form

$$u^+ = u^*/u_\tau = 2{\cdot}43 \ln (y^+) + 5{\cdot}0 + 2{\cdot}43\,\pi W(y/\delta), \qquad (5)$$

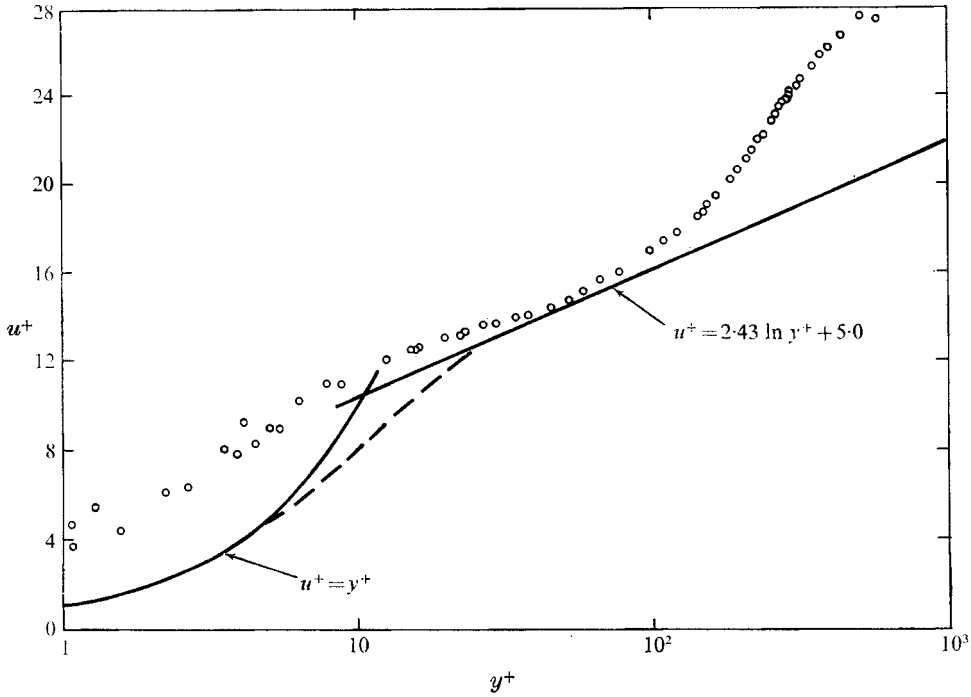

FIGURE 9. Correlation of the velocity profile in law-of-the-wake co-ordinates.

where $y^+ \equiv yu_\tau/\nu_w$, u_τ is the friction velocity, $\tilde{\pi}$ is a parameter representing the strength of the wake component of the boundary layer, ν_w is the kinematic viscosity, W is the Coles (1956) tabulated wake function, and u^* is the generalized velocity proposed by Van Driest (1951) to account for the effects of compressibility and heat transfer. The quantities u_τ, δ and $\tilde{\pi}$ are treated as unknown constants and are determined by adjusting their values until the data fits (5) with a minimum r.m.s. error.

The results of the correlation are shown in figure 9. The transformed velocities for $y^+ < 50$ were excluded from the data-fitting process, and are considerably larger than those predicted by the 'universal' correlation, reflecting the deviation from a linear profile that had been observed near the wall. In addition, the value of $\tilde{\pi}$ was found to be 1·4, slightly more than twice the value of 0·60 normally found in correlating zero-pressure-gradient flat-plate data and typical of flows with strong adverse pressure gradients (see Maise & McDonald 1968). On the other hand, the r.m.s. deviation of the velocity data used in the curve fit from the theoretical curve was 0·8%. Furthermore, the skin friction coefficient c_f was $4{\cdot}06 \times 10^{-4}$, which is within several per cent of the theoretical value determined from the Kármán–Schoenherr incompressible formula, using the $Re_\theta = 36\,800$ (calculated from the mean flow measurements), together with the Van Driest transformation functions, and following the procedure outlined by Hopkins & Inouye (1971). It appears, therefore, that the anomalous value of $\tilde{\pi}$ can be attributed primarily to the strong pressure gradient normal to the wall.

In summary, the probe measurements revealed a repeatable, two-dimensional

boundary-layer flow at high Reynolds number. The observed pressure rise of nearly 50 % from the layer edge to the wall is apparently a common phenomenon increasing with Mach number. Less typical of flat-plate boundary layers is the observed disagreement with the linear Crocco theory; however, the agreement with the incompressible law of the wake was good, and the experimental skin friction coefficient agreed with the theoretical value within several per cent. It should be noted, too, that the present data accounted for the observed gradient $\partial p/\partial y \neq 0$, although comparison was made with published data obtained by assuming $\partial p/\partial y = 0$.

Although the mean flow measurements extend to 0·010 in. (0·025 cm) from the wall, no indication of a linear variation of velocity in the sublayer was found. These measurements indicated that the sublayer was only 0·05 to 0·10 in. (0·12–0·25 cm) thick, which represents 1–2 % of the total boundary-layer thickness. The relatively thin sublayer has been attributed to the high Reynolds number Re_θ of the present study. The sonic line was found to occur at $y = 0{\cdot}5$ in. (0·12 cm), so that up to 50 % of the outer portion of the sublayer is supersonic. A more meaningful measurement of the sublayer geometry will be described in §5.

5. Intermittent boundary-layer structure

The intermittent structure of the boundary layer was measured separately from the mean and fluctuation properties, as a means of defining statistically the sublayer thickness and the boundary-layer 'front' (interface). The customary method was employed to assign the fluctuating portions of oscillograms to the turbulent flow and the fluctuation-free portions to the laminar flow. The turbulent contributions were then summed, and averaged by a special electronic circuit (Demetriades 1968*a*).

Several interesting features of the boundary-layer flow could be seen by observing the hot-wire signal at various y positions. For example, the signal 'one-sidedness' first reported by Kovasznay (1953) was observed to vary qualitatively as a function of y and hot-wire overheat. The hot wire is 'total-temperature sensitive' at the low overheats and 'mass-flux sensitive' at the high overheats; with a cooled wall, a hot wire located at the sublayer front alternates between regions of cold (in the T_0 sense), slow, laminar flow and regions of hotter, fast, turbulent flow. At low overheats (or currents i), the signal of this wire will therefore have 'spikes' (i.e. bursts of increasing wire voltage); at high overheats, the spikes reverse direction. The situation is exactly the opposite at the outer edge of the boundary layer proper, where the wire alternates between regions of cold, slow, turbulent fluid and regions of hot, fast laminar fluid. This 'double reversal', shown on figure 10 (plate 3), eases greatly the mechanics of the intermittency measurement.

The distribution of intermittency factor Ω in the boundary layer is shown in figure 11. Repeatability is emphasized by including all relevant data collected over a year of experimentation with a number of different hot wires at various overheats. Points are labelled by the number of the 'library' tape where they can be found. The r.m.s. sublayer thickness $\overline{\delta}_s$ and boundary-layer thickness $\overline{\delta}$ were

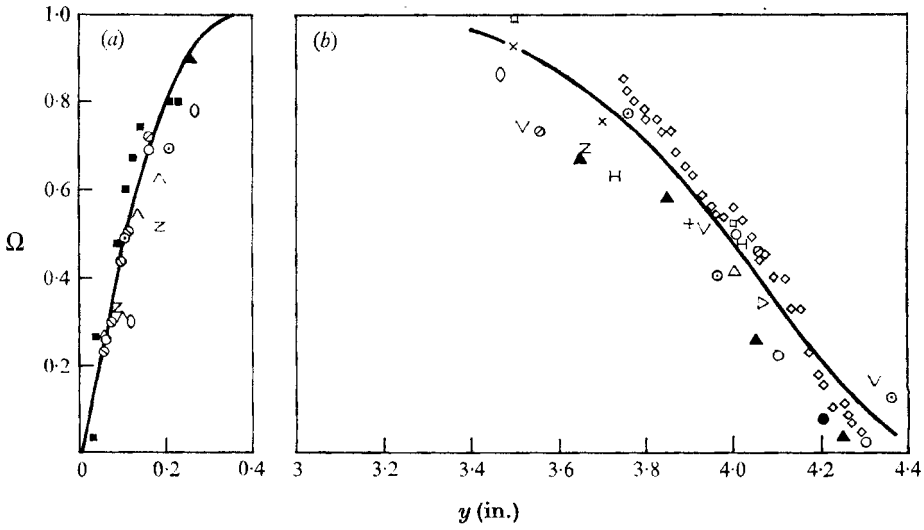

FIGURE 11. Intermittency distribution at the sublayer and boundary-layer fronts. (*a*) ——, empirical; (*b*) ——, fifth-degree polynomial (least squares).

	1971 data									1972 data								
Tape no.	23	21	22	24	25	27	28	30	31	32	33	34	17	18	26	35	36	37
	○	●	+	×	△	□	■	▲	⊘	⊘	○	∧	∨	H	▷	◊	Z	◇

found to be 0·125 and 4·05 in. (0·31 and 10 cm), respectively, and the standard deviations $d_s = 0{\cdot}075$ and $d = 0{\cdot}276$ in. (0·19 and 0·7 cm), respectively. The intermittency distribution deviates from 0 at the wall; the boundary-layer turbulence, therefore, occasionally reaches and touches the surface. At the outer edge, on the other hand, the front corrugations are given by $d/\bar{\delta} = 0{\cdot}068$, which is much smaller than the value $d/\bar{\delta} = 0{\cdot}18$ found by Klebanoff (1955) at $M_e = 0$. It is not presently clear whether this is a Mach number or a heat-transfer effect.

6. Turbulent fluctuations

Prior to decomposing the hot-wire signals into turbulence modes, it was necessary to account for limitations imposed by the characteristics of the instrumentation. The objective of this restoration procedure is to correct for known deficiencies in the frequency response of the measuring circuitry, including the hot-wire anemometer. If the transfer function (gain) of each component is a prescribed function of frequency f, then corrections to the data can be made easily when the gain is not unity in the frequency regime of interest. In the present case the 'boundary-layer frequency' $u_e/\bar{\delta} = 10$ kHz, and thus the frequency band, was limited arbitrarily to 200 kHz.† In this range the amplifier transfer function $G(f)$ was always unity. However, the hot-wire transfer function $W(f; t_w)$ is

† The choice was one of convenience. The 200 kHz limit was imposed by the FM bandwidth recording at 60 ips. It was not considered a major fault to limit the smallest eddies studied to $\bar{\delta}/20$.

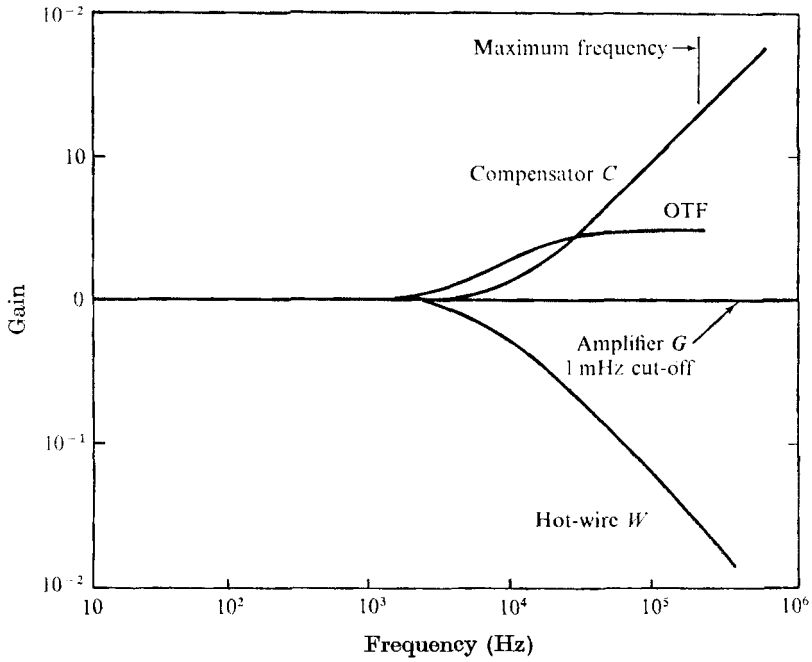

FIGURE 12. Typical transfer function of the hot-wire instrumentation. The curve labelled 'OTF' represents the overall transfer function of the instrumentation. Wire no. 6–3; A current; $y = 1{\cdot}02$ in.; $t_c = 16\,\mu$s.

additionally a function of its time constant t_w, which depended, in turn, on the probe location y and its heating current i. If t_w could be measured on every occasion, the corresponding time constant t_c of the compensating network with transfer function $C(f;t_c)$ could be electronically set at $t_c = t_w$; the compensation was then designed to give $C(f;t_c) = W(f;t_w)$.

Even if it were always possible to measure t_w, it would be impractically time-consuming This measurement was therefore made only once beyond the edge of the layer for each set of hot-wire measurements and t_c also put equal to the observed value t_{w1}. Then, as the hot wire was moved toward the wall, its time constant t_w varied (with y and i), so that $W(f;t_w)$ also changed in a way making it different from $C(f;t_c)$. The 'overall transfer function'

$$\text{OTF} \equiv [1/W(f;t_w)\,C(f;t_c)\,G(f)]^2 \tag{6}$$

therefore deviated from unity, typically as shown on figure 12. During data reduction, the t_w at any y and i was computed by

$$t_w = t_{w1}\left[\frac{R_1 i_1}{(\partial R/\partial i)_1}\frac{\partial R/\partial i}{Ri}\right]; \tag{7}$$

then W and thus the OTF were computed for this value. For each y and i, an 'error ratio'

$$J \equiv \int_0^\infty \text{OTF}\, e^2(f)\,df \Big/ \int_0^\infty (e(f)/G_0)^2\,df \tag{8}$$

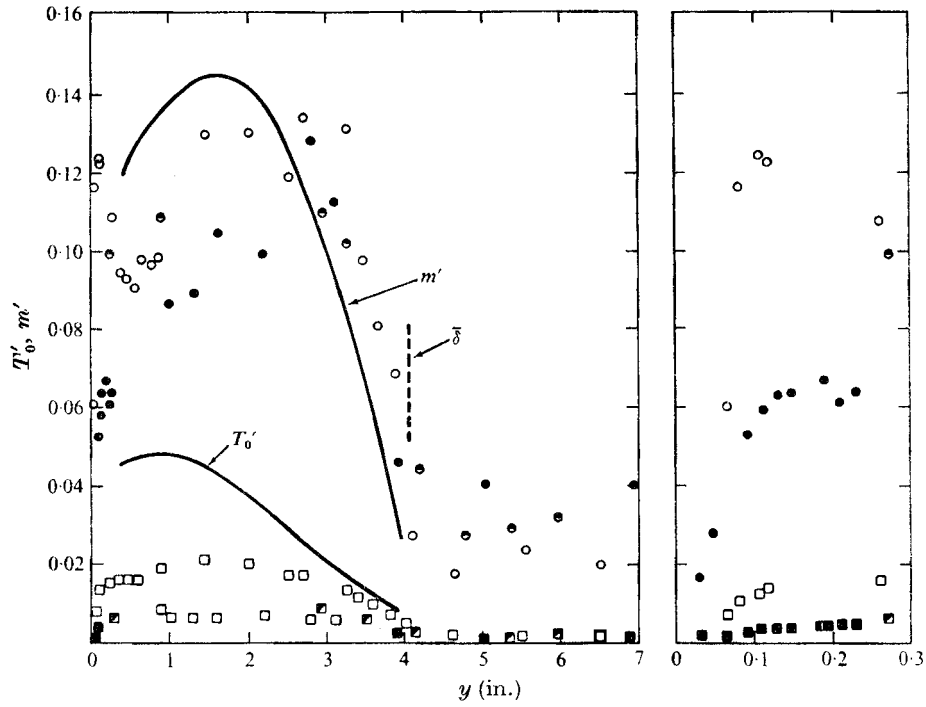

FIGURE 13. Variation of wideband r.m.s. mass-flux and total-temperature fluctuations across the boundary layer. Kistler's results at $M = 4{\cdot}76$ (solid line) are included for comparison.

m'	T_0'	Wire no.
○	□	A 13–1
●	■	6–3
◓	◩	2–5

was found next, where $e^2(f)$ is the spectrum of the measured hot-wire signal. The actual wide-band fluctuation of the hot-wire signal E_0^2 was next related to the measured signal by

$$E_0^2 = JE^2. \tag{9}$$

The corrected E_0^2 signals were then used in the modal analysis. Furthermore, the quantity OTF $e^2(f)$ is the corrected wire output spectrum, so that the response-restored spectrum is a direct by-product of the computation of J. In any case, the spectrum $e^2(f)$ of the hot-wire output is a necessary prerequisite for the extraction of the wide-band fluctuations, a central and not often appreciated point in applying hot-wire anemometry to compressible flows.

Following response restoration, the wide-band data were first reduced into the fluctuations m' in local mass flux and total temperature T_0'. The hot-wire sensitivity coefficients e_m and e_T, respectively, were determined by inserting into the formulae of Morkovin (1956) the wire calibration constants, and retaining only the Reynolds number derivatives of Nusselt number $\partial Nu/\partial Re$ and recovery factor $\partial\eta/\partial Re$. The results are shown in figure 13. It is noteworthy that the already large equilibrium (zero-current) hot-wire temperature was below the wire melting temperature sufficiently to allow ample artificial electrical heating. It is also noted

in figure 13 that two different hot wires (designated 6–3 and A13–1) produced virtually the same results. Figure 13 includes, too, Kistler's (1959) results, obtained at Mach 4·7. Although Kistler found that the fluctuation intensities m' and T_0' increased with increasing Mach number over the range from $M = 1{\cdot}7$ to $M = 4{\cdot}7$, the present results at $M = 9{\cdot}5$ are similar to Kistler's and, in fact, the peak total temperature fluctuation is only one-half Kistler's value. The fact that the present tests were conducted with a highly cooled wall while Kistler's data were acquired under adiabatic conditions represents a significant distinction between the two experiments.

Further decomposition of the hot-wire signals was made into the pressure, temperature, velocity and density fluctuations p', T', u' and ρ', respectively (here a prime denotes the local wide-band root-mean-square fluctuation divided by its corresponding mean value). Using the notation of Morkovin (1956), the corresponding instantaneous normalized fluctuations of the entropy, vorticity and sound are related to the flow fluctuations by

$$\sigma = \Delta T/T - ([\gamma-1]/\gamma)\,\Delta p/p, \quad \tau = \Delta u/u - (n_x/\gamma M)\,\Delta p/p, \quad \pi = \Delta p/\gamma p, \tag{10}$$

where it has been assumed that the sound waves sensed by the hot wire are planar with direction cosine n_x and the r.m.s. mode fluctuations are again denoted by prime, e.g. $\sigma' = [\overline{\sigma^2}]^{\frac{1}{2}}$.

It is well known that such a complete 'modal split' is formally impossible with a hot wire, because its response equations, even in the linearized case, are mathematically under-determined. For compressible turbulent flows in the range $M < 5$ it had been previously assumed that $p' = 0$ (Kistler 1959; Demetriades 1968*b*), in which case the equations become determinate and $\sigma' = T'$, $u' = \tau'$. The $p' = 0$ assumption was also used here to make a 'first-order' computation of T' and u'; the results will not be presented, since they were, somewhat surprisingly, approximately the same as those obtained below for $p' \neq 0$. That the $p' = 0$ assumption was invalid in the present case became clear when estimates made of p' at the wall ($y = 0$) and in the free stream ($y > \bar{\delta}$), by extrapolating the published findings of Kistler & Chen (1964), gave $p'(y = 0) = 10$–$15\,\%$ and $p'(y > \bar{\delta}) = 3\,\%$. These were large compared with the computed u' ($p' = 0$), and therefore cast serious doubt on the assumption $p' = 0$ within the layer itself.

An alternative reduction of the data was therefore made by retaining p', in which case the modal equation for the fluctuations u', T', p' and the cross-correlations R_{uT}, etc., became

$$Y^2 = T'^2 + u'^2X^2 + \left[\frac{\beta-\alpha X}{\beta+\alpha}\right] p'^2 + 2u'T'R_{uT}X - 2\left[\frac{\beta-\alpha X}{\beta+\alpha}\right][T'p'R_{Tp} - u'p'R_{up}X], \tag{11}$$

where the 'modal variables' X, Y and the Mach-dependent constants α, β are the classical notation given by Morkovin (1956). An equation equivalent to (11) for the turbulence modes of vorticity τ', entropy σ' and sound π' could be written

$$Y^2 = \sigma'^2 + \tau'^2X^2 + [f(M) + g(M, n_x)\,X]^2\pi'^2 + 2\sigma'\tau'R_{\sigma\tau}X + 2[f(M) + g(M, n_x)]\,[\sigma'\pi'R_{\sigma\pi} + \tau'\pi'R_{\tau\pi}X]. \tag{12}$$

	Data reduction scheme	Consequence
(i)	$R_{up} = R_{pT} = R_{uT} = 0$	Implies $p' = 0$
(ii)	$R_{\tau\pi} = R_{\sigma\pi} = R_{\sigma\tau} = 0$	No solution in boundary layer
(iii)	$R_{\sigma\pi} = R_{\tau\pi} = 0$, $R_{\sigma\tau} = -1$	Solution physically possible
(iv)	$R_{\sigma\pi} = R_{\tau\pi} = 0$, $R_{uT} = -1$	$\lvert R_{\sigma\tau}\rvert > 1{\cdot}0$
(v)	$R_{Tp} = R_{pu} = 0$, $R_{uT} = -1$	Implies $p' = 0$

TABLE 2. Summary of assumptions made in §6.

To solve either (11) or (12) for p', T', u', σ', etc., in the case of finite pressure fluctuations, it is necessary to specify the direction cosine n_x. Following Kovasznay's argument (1953) that the hot wire is most sensitive to sound waves which are almost Mach waves, we make this assumption, so that $n_x = -1/M$. Equations (11) and (12) were then solved subject to specific assumptions concerning the cross-correlation terms. For example, although Laufer's (1964) measurements at supersonic speeds indicated that, in the free stream, the sound field dominated the other modes, the free-stream mode diagram obtained in the present experiment clearly showed the co-existence of several modes. Laufer's experiments were performed in an unheated wind tunnel, in which case it can be reasoned that the free-stream vorticity and entropy fluctuations would not be significant. The present experiment, however, was carried out at elevated stagnation temperatures, and temperature spottiness produced by the tunnel heaters could be expected to persist in the test section free-stream flow. Kovasznay (1953) suggests that for a 'good' wind tunnel, the modes originate at different regions, and would therefore co-exist in an uncorrelated fashion. Therefore, it was first assumed that $R_{\sigma\tau} = R_{\sigma\pi} = R_{\tau\pi} = 0$, and (12) was solved for the r.m.s. mode fluctuations. In an analogous fashion, it was also assumed that $R_{uT} = R_{up} = R_{Tp} = 0$†, and (11) was solved for the r.m.s. fluctuations of the flow variables, to yield a second alternative to the 'no sound' solution.

Within the boundary layer it is expected that the modes would be correlated to some degree. However, Morkovin (1956) points out that, since the manner of sound propagation is basically so different from that of vorticity and entropy, the coefficients $R_{\sigma\pi}$ and $R_{\tau\pi}$ are generally negligible or zero. Furthermore, the results of the 'first-order' no-sound assumption indicated that $R_{\sigma\tau}$ is very close to -1, and it was not expected that the value of this parameter would change significantly in the presence of finite pressure fluctuations. Thus, several solutions were also attempted with $R_{\sigma\pi} = R_{\tau\pi} = 0$ (or $R_{up} = R_{Tp} = 0$) and with either $R_{\sigma\tau}$ or $R_{uT} = -1$. No attempt was made to test the sensitivity of the results to small variations in $R_{\sigma\tau}$.

A summary of the various assumptions described above, and the consequences of their selection, are listed in table 2. The uncorrelated-modes assumption ((ii), table 1) leads to a solution only in the free stream, where a pressure fluctuation of several per cent was obtained. Of the remaining schemes, only assumption (iii) with $R_{\sigma\pi} = R_{\tau\pi} = 0$, $R_{\sigma\tau} = -1$ yields a physically plausible solution through

† Since both velocity and temperature fluctuations are induced by the pressure fluctuations, this assumption is strictly valid only when p' becomes vanishingly small.

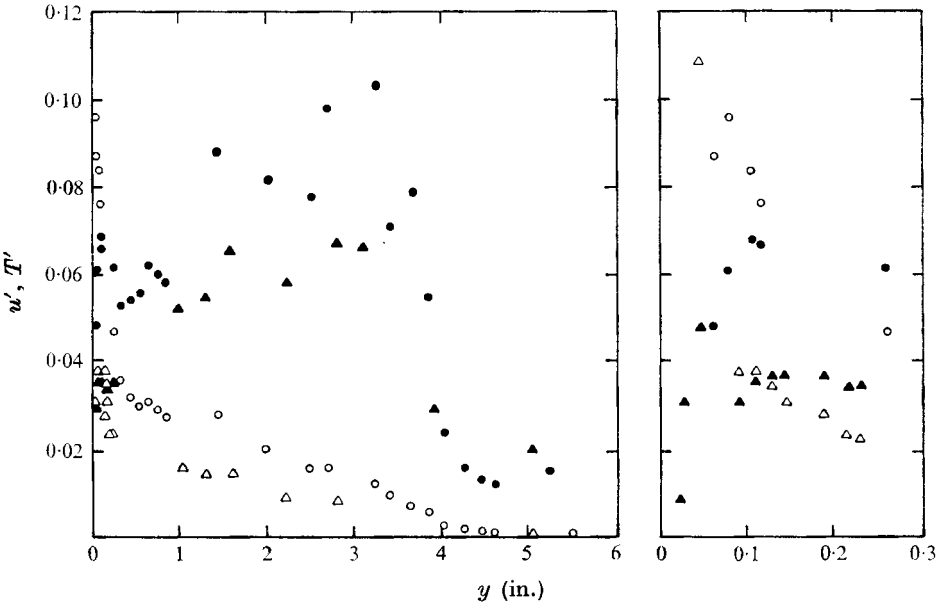

FIGURE 14. Variation of wide-band r.m.s. velocity and temperature fluctuations across the boundary layer. $p' \neq 0$.

u'	T'	Wire no.
○	●	A 13–1
△	▲	6–3

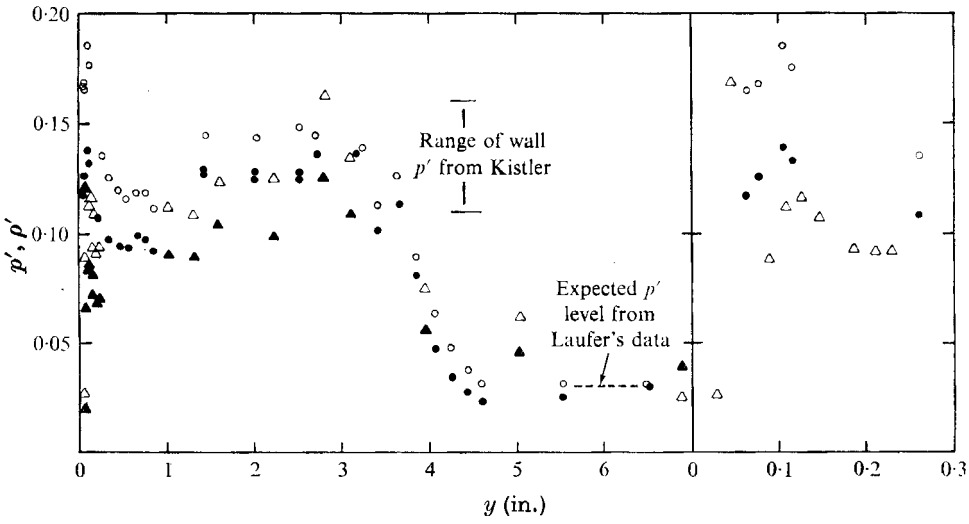

FIGURE 15. Variation of wide-band r.m.s. pressure and density fluctuations across the boundary layer. $p' \neq 0$.

p'	ρ'	Wire no.
○	●	A 13–1
△	▲	6–3

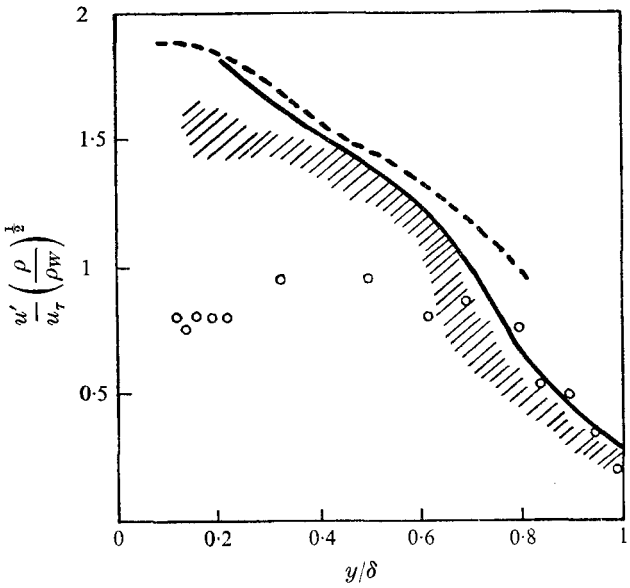

FIGURE 16. Correlation of wide-band longitudinal velocity fluctuations based on friction-velocity scheme for compressible flow. ○, present results; ////, Kistler (1959); —, Klebanoff (1955); - - -, Morkovin & Phinney (1958).

the boundary layer. Detailed results arising from this assumption are presented directly below.

The wide-band fluctuation magnitudes are shown on figures 14 and 15. It is seen that the boundary-layer fluctuations are dominated by p', while at the other extreme the longitudinal turbulence component u' is very small. It is remarkable that the p' component fits smoothly the levels at the wall and free stream extrapolated for $M_e = 9{\cdot}4$ from, respectively, the data of Kistler & Chen (1963) and Laufer (1964). Peaks in the intensity distribution are obtained in the middle of the layer and again at the sublayer edge. The latter, however, is due most probably to the sublayer intermittency, i.e. to the alternating exposure of the hot wire to consecutive stretches of laminar and turbulent flow. The prominence found of the pressure fluctuations seems to vindicate the earlier postulates (Laufer 1968) of fundamental changes in the nature of the boundary layer above M_e of about 5. In the same manner, the comparison shown on figure 16 of the velocity fluctuations with earlier data, reduced according to a scheme suggested by Morkovin (1962), shows a lower u' level than expected. One is tempted to attribute this turbulent kinetic energy loss to the sound radiation escaping from the boundary layer into the free stream.

There is seeming agreement of the measured T' as plotted in figure 17 with the data of Kistler, especially when the 'driving force' is taken to be the difference between the wall and external temperatures. However, the ratio $T'/(\gamma-1)\,M^2u'$, plotted in the same figure, shows that the 'strong Reynolds analogy'

$$T' = (\gamma-1)\,M^2u'$$

weakens considerably in the presence of heat transfer.

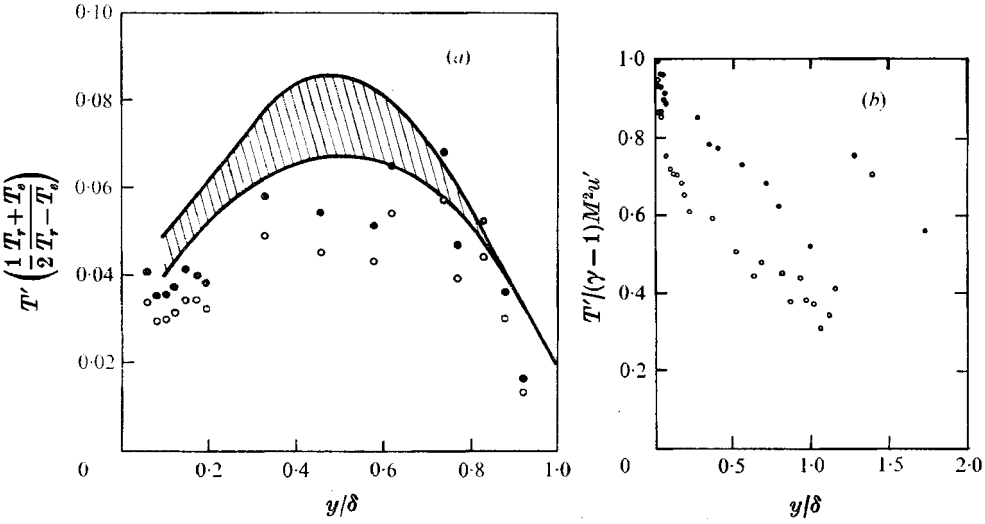

FIGURE 17. Correlation of wide-band static temperature fluctuations in supersonic–hypersonic boundary layers. (*b*) shows departure from strong Reynolds analogy caused by heat transfer to the wall. (*a*) ▨, Kistler data range; ○, $T_r = T_0$; ●, $T_r = T_w$. (*b*) ○, wire no. A 31–1; ●, 6–3.

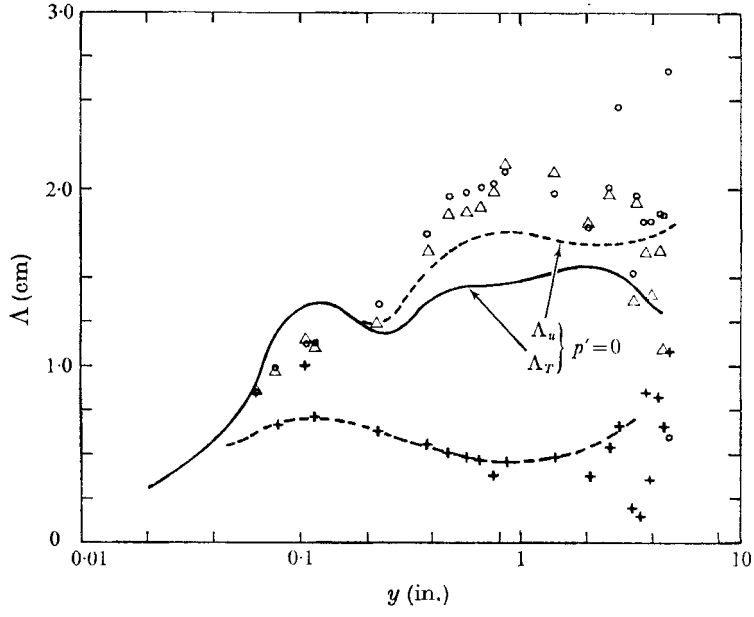

FIGURE 18. Longitudinal integral scales of velocity, temperature and pressure transformed from the corresponding time scales by using the local mean flow speed. Curves marked $p' = 0$ show differences found when the 'no-sound' assumption is made. ○, Λ_u; △, Λ_T; +, Λ_p.

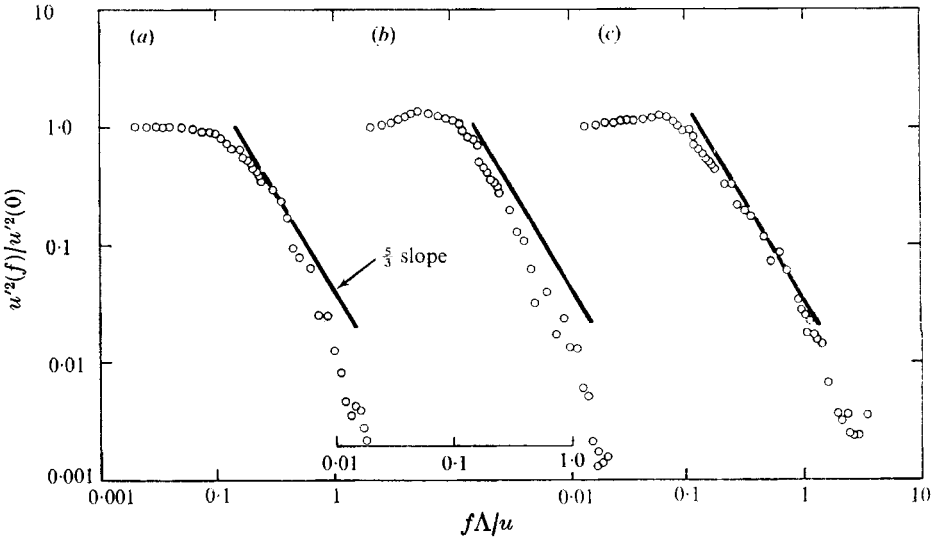

FIGURE 19. Typical spectra of turbulent longitudinal velocity fluctuations at three representative locations within the boundary layer

	(*a*)	(*b*)	(*c*)
$y/\bar{\delta}$	0·0316	0·101	0·84
Re_Λ	400	800	5000

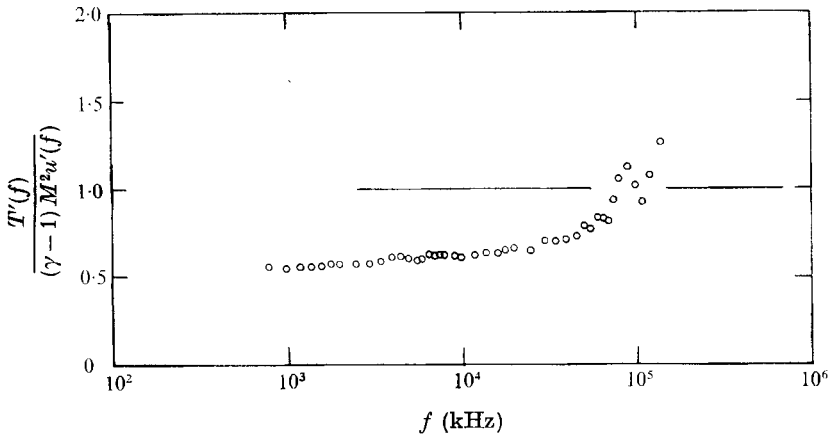

FIGURE 20. Spectral dependence of the ratio of temperature to velocity fluctuations at a typical location in the boundary layer.

The longitudinal integral length scales were inferred from the modally resolved spectra by invoking Taylor's hypothesis of frozen convection. For all turbulence modes, excepting the pressure, the scales are the same in magnitude, reaching approximately $\Lambda \simeq \frac{1}{5}\bar{\delta}$ toward the edge of the layer; the pressure scales are considerably smaller. However, the time-to-length transformation for all length scales plotted in figure 18 was made using the local mean flow velocity, clearly an improper assumption for the sound mode. The turbulent spectra were also resolved, as noted above, into their respective modes at each point, and typical instances are shown in figure 19. There is an increasing tendency towards an

inertial subrange as one proceeds towards the edge of the layer. This can be attributed to an increase of the turbulence Reynolds number $Re_\Lambda = \overline{u}u'\Lambda_u/\nu$, which varies from about 500 at the sublayer edge ($y/\overline{\delta} \simeq 0{\cdot}025$) to 5000 in the middle of the layer ($y/\overline{\delta} \sim 0{\cdot}5$).

The resolution of the spectra into their turbulence mode components allows one further insight into the effect of heat transfer. The question can be posed as to which Fourier component is responsible for the 'weakness' of the Reynolds analogy $T' = (\gamma - 1)M^2u'$, shown in figure 17. According to figure 20, the temperature fluctuations T' are abnormally low for the larger eddies which, of course, are mainly responsible for communicating the wall conditions to the free-stream and vice versa. Conversely, then, it seems that the cooled-wall condition is largely responsible for departure from the 'strong Reynolds analogy', i.e. for

$$T' \neq (\gamma - 1)M^2u'.$$

7. Conclusions

In summary, the hypersonic turbulent boundary layer examined was in all respects normal, including the apparently Mach number induced pressure gradient along y, except possibly for the nonlinear velocity variation in the sublayer. The front or interface of the latter was clearly detected, and the standard front deviation of the boundary layer proper was found to be much smaller than that encountered in incompressible boundary layers. Large pressure fluctuations accompanied by diminished velocity fluctuations were found, and there is evidence that the sound radiated to the surface and to the external stream agrees with extrapolation of data at lower Mach number. The integral scales reach $\frac{1}{6}\overline{\delta}$, contributing to large turbulence Reynolds numbers and thus to the existence of an inertial subrange in the turbulent spectra. The temperature fluctuations agree with predictions based on adiabatic supersonic boundary layers, but apparently only because they are suppressed by wall cooling. In this respect, a study of the effect on T' of Mach number, isolated from the effect of heat transfer, would be an interesting extension of this work.

Quite separately, this work demonstrated the utility of the hot-wire anemometer for quantitative turbulence measurements at hypersonic speeds. Such probes were routinely operated at 1000 °F (800 °K) and 5 cm Hg dynamic pressure, with a frequency response easily exceeding the corresponding demands of the turbulent flow. The indeterminancy of the anemometer signal was circumvented by rejecting, on a trial-and-error basis, physically and mathematically implausible solutions. However, future research in this area with the hot-wire anemometer will require increased attention to the technique by which the turbulence modes are separated.

The authors acknowledge the assistance of Lee Von Seggern, who was responsible for the electronic instrumentation, and E. L. Doughman, who prepared the hot-wire anemometer probes. This work was supported by ARPA, and primarily by the USAF Space and Missile Systems Organization under contracts FO4701-70-C-0130 and FO4701-71-C-0035.

REFERENCES

BEHRENS, W. 1963 *A.I.A.A. J.* **1**, 2864.

COLES, D. 1956 *J. Fluid Mech.* **1**, 191.

COLES, D. 1969 *Proc. AFOSR-IFP Conf. on Computation of Turbulent Boundary Layers*, Stanford University, vol. 2 (ed D. Coles and E. Hirst).

DEMETRIADES, A. 1968*a* *J. Fluid Mech.* **34**, 465.

DEMETRIADES, A. 1968*b* *Phys. Fluids*, **11**, 1841.

DOUGHMAN, E. L. 1972 *Rev. Sci. Instr.* **43**, 1200.

FELLER, W. V. 1973 *A.I.A.A. J.* **11**, 556.

HOPKINS, E. J. & INOUYE, M. 1971 *A.I.A.A. J.* **9**, 993.

KANE, E. D. & MASLACH, G. I. 1950 *N.A.C.A. Tech. Note*, no. 2210.

KEMP, J. H. & OWEN, F. K. 1972 *N.A.S.A. Tech. Note*, *D*-6965.

KISTLER, A. L. 1959 *Phys. Fluids*, **2**, 290.

KISTLER, A. L. & CHEN, W. S. 1963 *J. Fluid Mech.* **16**, 41.

KLEBANOFF, P. S. 1955 *N.A.C.A. Tech. Rep.* no. 1247.

KOVASZNAY, L. S. G. 1950 *J. Aero. Sci.* **17**, 565.

KOVASZNAY, L. S. G. 1953 *J. Aero. Sci.* **20**, 657.

LAUFER, J. 1964 *Phys. Fluids*, **7**, 1191

LAUFER, J. 1968 *N.A.S.A. Special Paper*, no. 216.

LEE, R. E., YANTA, W. J. & ZEONAS, A. C. 1969 *Naval Ordnance Lab. Rep.* TR 69–106.

MAISE, G. & MCDONALD, H. 1968 *A.I.A.A. J.* **6**, 73.

MATHEWS, M. L. 1958 *Guggenheim Aero. Lab. California Institute of Technology, Hypersonic Res. Memo.* no. 44.

MORKOVIN, M. V. 1956 *AGARDograph*, no. 24.

MORKOVIN, M. V. 1962 *La Mécanique de la Turbulence*, p. 367. Paris: C.R.N.S.

MORKOVIN, M. V. & PHINNEY, R. E. 1958 *Johns Hopkins University Rep.* AFOSR TN-58–469.

ROGERS, K. W., WAINWRIGHT, J. B. & TOURYAN, K. J. 1966 *Rarefied Gas Dynamics*, vol. 2, suppl. 3 (ed. J. H. DeLeeuw), p. 151. Academic.

VAN DRIEST, E. R. 1951 *J. Aero. Sci.* **18**, 145.

WALZ, A. 1962 *La Mécanique de la Turbulence*, p. 399. Paris: C.N.R.S.